THE JOURNAL OF PHYSICAL CHEMISTRY C

Article

pubs.acs.org/JPCC

Multifunctions of Net Surface Charge in the Reaction on a Single Nanoparticle

Shaobo Xi[†] and Xiaochun Zhou*[,†,‡]

[†]Division of Advanced Nanomaterials, and [‡]Key Laboratory of Nanodevices and Applications, Suzhou Institute of Nano-Tech and Nano-Bionics, Chinese Academy of Sciences, Suzhou 215125, China

Supporting Information

ABSTRACT: Electric charge can determine where and how reaction occurs, but the relationship between net surface charge and activity is unclear because of the difficulty in simultaneously detecting charge and activity at the single nanoparticle level. In this study, we use ions as probes to detect the distribution of net surface charge and track galvanic replacement reaction on single Ag nanowire in situ and in real time by dark-field microscopy. The two ends of a single Ag nanowire are found to possess more net surface charges than the middle part. The unevenly distributed net surface charge performs multifunctions in determining the reaction activity, selectivity, and product shape. Owing to the interaction between the net surface charges and ions in solution, many clusters are generated on the Ag nanowires. The locations of generating these clusters are where faster deposition reaction happens. Furthermore, larger size Ag compounds with clear shape are produced near the two ends by attracting Ag^+ at lower [$HAuCl_4$], but larger size Ag−Au alloy clusters with veiled shape are produced near the center by repelling $AuCl_4^-$ at higher [$HAuCl_4$]. Given that net surface charge generally exists in nanoscience, the methodology and results obtained from this research can be widely used in other single-shaped nanomaterials.

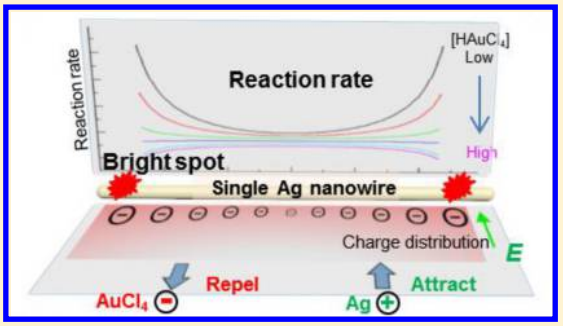

1. INTRODUCTION

Electric charge can determine where and how reaction occurs. The surface of a conductive material in solution could carry certain charges through several modes, such as electron affinity (i.e., electrochemical potential) differences of two phases, ionization of surface groups, differential ion adsorption from electrolyte solution, and differential ion dissolution from a crystal lattice.[1−3] Opposite charges will be attracted to the interface between the conductive material and solution, automatically forming an electric double layer. Within the electric double layer only, the net surface charges can interact with other charged objects, such as ions, colloidal particles, and electrons.[1] Given that nanoparticles possess different shapes and structures, the distribution of net surface charge on a single nanoparticle usually presents diverse patterns.[4,5] This unevenly distributed net surface charge could generate a specific electric field or potential around conducting materials and affect the transportation of charged reactants and their corresponding reactions.[6−12] Ultimately, the net surface charge can determine the preferred location for chemical reactions on a single nanoparticle.[13,14]

However, a clear relationship between the net surface charge and reaction has not been well established at the single nanoparticle level.[13−16] This problem is due to the difficulty of simultaneously detecting the distribution of net surface charge and the effect on reaction at the single nanoparticle level. Electric force microscopy (EFM) is currently the most effective technique to measure the distribution of net surface charge with nanometer accuracy.[17] But the reaction on the nanomaterial in situ and in real time is difficult to measure by using EFM. Moreover, measuring the distribution of net surface charge in solution remains a challenging work for this technique.[18]

Galvanic replacement reaction (GRR) is a powerful method in engineering metal nanostructures in numerous fields, including catalysis,[19] plasmonics,[20] and biomedical research.[21] GRR is also an excellent model reaction system for studying the effect of net surface charge on reaction, as GRR is a simple electrochemical process. For a typical GRR between Ag and $HAuCl_4$, two half-reactions occur:

$$Ag - e^- \rightarrow Ag^+ \qquad \varphi^{\ominus}_{Ag/Ag^+} = 0.799\ V \tag{1}$$

$$AuCl_4^- + 3e^- \leftrightarrow Au\downarrow + 4Cl^- \qquad \varphi^{\ominus}_{Au/AuCl_4^-} = 1.000\ V \tag{2}$$

GRR between the Ag nanoparticle/nanowire and $HAuCl_4$ has been intensively studied by Sun and Xia.[21−30] It is accepted that the replacement occurs through the Au deposition on the surface of the nanoparticle/nanowires. Then some pits with irregular shapes and surfaces are formed on the surface because some spots on the surface usually exhibit higher surface energy originating from crystalline defects such as steps and dislocations. As a result of the formation of the pits, $HAuCl_4$

Received: December 18, 2015
Revised: July 1, 2016
Published: July 11, 2016

DOI: 10.1021/acs.jpcc.5b12390
J. Phys. Chem. C 2016, 120, 16608−16616

solution can corrode the inner part of the nanostructure, inducing the formation of the hollow structure.[9,11]

Ag and Au are plasmonic materials, which are amenable to optical probing at the single particle level.[31] Dissolution of Ag will induce a decrease in light scattering, whereas Au deposition will cause an increase. In this work, we conducted a challenging study on net surface charge and determined its effect on GRR at the single nanoparticle level. The results revealed that the two ends of a single Ag nanowire possess more net surface charges, and the unevenly distributed net surface charge performs multifunctions for the GRR on single Ag nanowire.

2. EXPERIMENTAL SECTION

2.1. Materials and Characterizations. All commercial materials were used as received unless specified. Transmission electron microscopy (TEM), scanning TEM (STEM), high-resolution TEM (200 kV, Tecnai G2 F20 S-TWIN; FEI), scanning electron microscopy (SEM, Quanta 400 FEG; FEI), and energy-dispersive X-ray (EDX) spectroscopy were used to characterize the nanostructure and composition of silver nanowires. These techniques were performed at CAS-Platform for Characterization and Testing at the Suzhou Institute of Nano-Tech and Nano-Bionics. Image analyses were conducted using home-written SCILAB codes.

2.2. Synthesis of Ag Nanowires. Silver nanowires were synthesized following the method of Xia et al.[28] In a typical synthesis, 0.1 mol of NaCl (Enox, China) and 2.24 g of poly(vinylpyrrolidone) (MW = 1 300 000) (Aldrich) were added to ethylene glycol (EG) (Sinopharm Chemical Reagent Co., Ltd.) and heated to obtain a clear solution. $AgNO_3$ (The First Regent Factory, Shanghai, China) solution (0.1 M, in EG) was added dropwise to the solution with vigorous stirring for 10 min. The mixed solution was poured into a Teflon-lined stainless-steel autoclave and was heated at 160 °C for 6 h. The product was diluted with ethanol and centrifuged several times at 2000 rpm for 5 min to remove the surfactant. Finally, the purified nanowires were dispersed in ethanol (Sinopharm Chemical Reagent Co., Ltd.).

2.3. Electrochemical Potential Measurements of Ag Nanowires during the GRR. All experiments were conducted at room temperature under ambient conditions.[4] All electrochemical potentials were measured at open circuit condition in CS350 potentiostat/galvanostat (Wuhan CORRTEST Instruments Co., Ltd.) with a three-electrode cell. The reference electrode is the Ag/AgCl/sat. KCl reference electrode. All potentials were quoted with respect to RHE reference electrode for comparison. The counter electrode was a large area Pt plane. The Au electrode was polished with a slurry of 0.05 μm alumina powders (CH Instruments, Inc.) and sonicated in water.

The working electrode is some Ag nanowires, which are supported on a bare Au electrode with a diameter of 2 mm (CH Instruments, Inc.). The Ag nanowires were immobilized by dropping 2 μL of Ag nanowire colloidal solution onto the bare Au electrode. Then the electrode was dried in air for 20 min. The Ag nanowires on Au electrode were immersed in 15 mL of $HAuCl_4$ solution for open circuit potential (OCP) measurement. Since the amount of $HAuCl_4$ was much larger than Ag nanowire, the GRR could not obviously change the concentration of $HAuCl_4$.

2.4. Dark-Field Imaging of Single Ag Nanowires. Dark-field measurements were performed using an Olympus IX71 microscope. The single Ag nanowires were illuminated by a cold white collimated LED (MCWHL2-C1) lamp source for Olympus BX & IX focused through an Olympus U-DCW NA1.2-1.4 oil immersion dark-field condenser. The scattering signal was collected by a 60× NA1.2 water-immersion objective and detected by an ANDOR Ixon DU-897D-CS0-#BV EMCCD camera operated at 200 ms frame rate. An additional 1.6× magnification on the microscope was also used. To correct the unavoidable stage drifting in nanometer accuracy[32−34] (Figure S5), we used super-resolution microscopy to localize accurately the markers, i.e., several gold nanoparticles with a size of tens of nanometers. As a result, the calculation of light scattering from single Ag nanowires can be highly improved.

2.5. Dark-Field Imaging of GRR on Single Ag Nanowires. A 100 μm (height) × 2 cm (length) × 5 mm (width) flow cell, which was formed by double-sided tapes sandwiched between a glass slide (Henghao, China) and a borosilicate coverslip (Citoglas, China), was used to hold aqueous reactant solutions for dark-field measurements. Reactant solutions were supplied in continuous flow at 10 μL min^{-1} by using a syringe pump. All dark-field imaging experiments on nanoparticle catalysis were carried out at room temperature with 0.02, 0.05, 0.10, and 0.50 mM $HAuCl_4$ (Nanjing Precious Metal Factory, China). This flow cell-based reactor provided a steady-state reaction condition. All GRR kinetics of single Ag nanowires was measured under this condition.

To immobilize Ag nanowires on the glass slide, we first dispersed 2 μL (depending on the concentration of Ag nanowire) of Ag nanowires in 20 μL of ethanol by sonication. A 5 μL volume of this solution was drop-cast once onto a clean glass slide and dried in air at room temperature. The glass slide was then assembled into a flow cell for dark-field imaging experiments.

2.6. Drift Correction by Super-Resolution Microscopy. Several gold nanomarkers were immobilized on the surface of the glass slide to accomplish drift correction. These gold nanomarkers could keep scattering the light and were highly stable during GRR. Therefore, the gold nanomarkers were not affected by the reactant solution. Super-resolution microscopy, which is similar to STORM,[35] PALM,[36] and our research,[32,37] was applied to localize the position of individual nanomarkers in nanometer accuracy.

To determine the emission center of the marker during the GRR, we cropped an image area of 13 × 13 pixels (~2.2 × 2.2 μm^2) around the nanomarker for 2D Gaussian fitting. To increase the accuracy of fitting, several frames (every 18th frame here) were combined to form a single image to gather a sufficiently large number of emission photons for analysis. As the pixel size of the combined image was only 166.67 nm, the image was fitted with a 2D Gaussian function to achieve subdiffraction accuracy.

3. RESULTS AND DISCUSSION

3.1. Measure the Activity of GRR on Single Ag Nanowires by DFM. The prepared Ag nanowires (50.1 ± 8.5 nm diameter and 6.3 ± 3.6 μm length; Figure 1A and Figure S1)[28] were well-dispersed and immobilized on a glass slide. The slide was then fabricated to a microfluidic flow cell for dark-field measurements in Figure 1B. Figure 1A shows that the as-synthesized Ag nanowire possesses a smooth edge and consequently shows an even scattering intensity in DFM (Figure 1C).

DOI: 10.1021/acs.jpcc.5b12390
J. Phys. Chem. C 2016, 120, 16608−16616

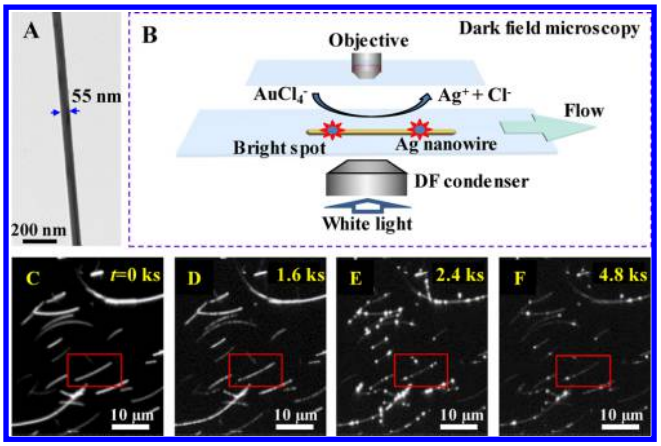

Figure 1. Imaging GRR on single Ag nanowires by DFM: (A) TEM image of a segment of an as-synthesized Ag nanowire; (B) schematic of GRR under DFM; (C−F) wide-field images of the nanowires from DFM under GRR at 0.02 mM $HAuCl_4$ at the time 0, 1.6, 2.4, and 4.8 ks from Movie S1.

Parts C−F of Figure 1 show the DFM scattering snapshots of some single Ag nanowires undergoing GRR during 0−4.8 ks. Figure 1D shows that single Ag nanowires become less bright after ∼1.6 ks GRR because of the dissolution of Ag nanowire through the oxidation half-reaction in eq 1. Interestingly, numerous bright spots with increased scattering intensity are generated on several locations of the single Ag nanowires at ∼2.4 ks (Figure 1E). These locations of Ag nanowires on the bright spots obviously have higher activity for the deposition reaction than other locations. Thus, in this study, DFM can effectively differentiate and measure the two half-reactions of GRR, i.e., reactions in eq 1 and eq 2, on single Ag nanowires. Our research is focused on the reduction half-reaction, as the half-reaction involves the reduction of ions from solution and is easily affected by the net surface charge.

3.2. Diverse Activity Distributions on a Single Ag Nanowire at Different Concentrations of $HAuCl_4$ ($[HAuCl_4]$).

To deeply study the GRR process on single Ag nanowire, we cropped two typical single Ag nanowires from the whole images taken at low (0.02 mM) and high (0.50 mM) $[HAuCl_4]$ during GRR, respectively. Parts A−C of Figure 2 show the variation of scattering intensity in different manners for a typical single Ag nanowire during GRR at 0.02 mM $[HAuCl_4]$ (red rectangle in Figure 1). Parts A−C of Figure 2 show that the intensity along the nanowire is almost uniform at the beginning of GRR. At 1.6 ks, the intensity increases at certain locations (e.g., L1, L2, L4) but decreases at others (e.g., L3). Several bright spots appear along the nanowire between 1.6 and 2.4 ks. Figure 2C shows that the exact appearance time of the bright spots is at ∼1.8 ks. During the same time, the scattering intensity of each location on the single Ag nanowire suddenly decreases to an extremely low value. It indicates that the brightening of the bright spots is at the expense of decreasing the scattering intensity of other locations on the nanowire. After 2.4 ks, the intensity of bright spots becomes increasingly lower until it disappears. Moreover, the locations of the bright spots are closer to the two ends of single nanowires at low $[HAuCl_4]$ (Figure 1E and Figure 2A−C).

The reaction behavior at high $[HAuCl_4]$ is different from that at low $[HAuCl_4]$. Parts D−F of Figure 2 show that the bright spots appear only after 30 s of the reaction at high $[HAuCl_4]$ (Movie S2). Moreover, the scattering intensity at every location (no matter with or without bright spots) of nanowire keeps increasing after 30 s (Figure 2E and Figure 2F). The increase of scattering intensity may be due to the continuous deposition of Au and reconstruction of the nanoparticles via Ostwald ripening. Both the continuous deposition of Au and Ostwald ripening can make the morphology change of the nanowire, resulting in the increase of the scattering intensity.[29] Figure 2E shows that more bright spots appear in the middle part of nanowire compared to Figure 2B. Therefore, the bright spot on the single Ag nanowire could show diverse distributions at different $[HAuCl_4]$s.

3.3. Structure and Composition of the Product at Different $[HAuCl_4]$s.

The structure and composition of typical

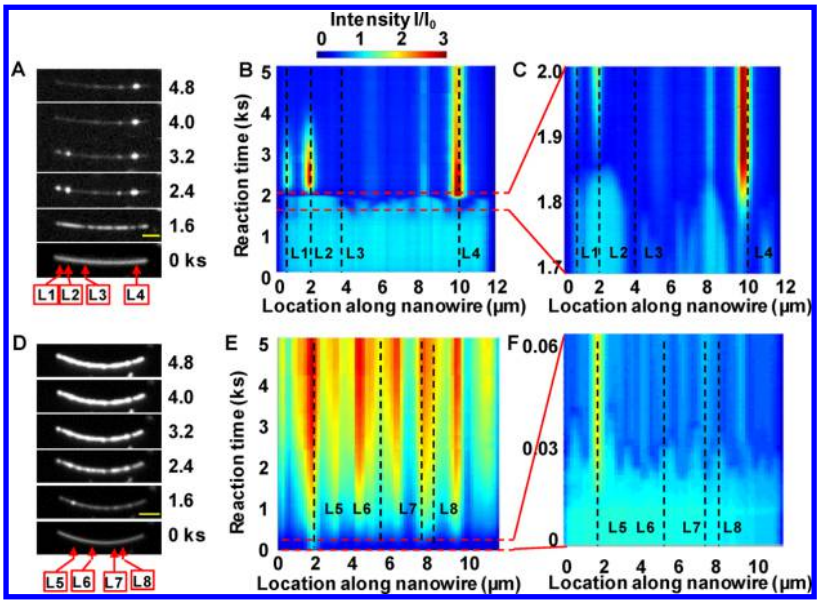

Figure 2. Typical DFM images and corresponding intensity of single Ag nanowires during GRR at different $[HAuCl_4]$s. (A) and (D) Typical DFM images of one single Ag nanowire during GRR at 0.02 and 0.50 mM $HAuCl_4$. Scale bar in parts A and D is 2 μm. (B, E) 2D light scattering intensity versus time along the Ag nanowire in parts A and D, respectively. (C, F) Zoom in of parts B and E.

DOI: 10.1021/acs.jpcc.5b12390
J. Phys. Chem. C 2016, 120, 16608−16616

single nanowires were characterized after GRR at different [$HAuCl_4$]s. Figure 3A shows that several large blocks, i.e.,

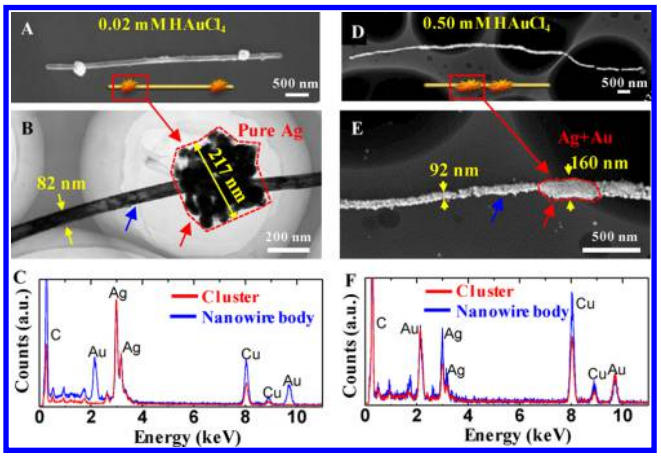

Figure 3. Structure and composition of typical single Ag nanowires after 2.4 ks of GRR at different [$HAuCl_4$]s: (A) SEM image of a single Ag nanowire at 0.02 mM $HAuCl_4$; (B) TEM image of a bright spot; (C) EDX measurement of nanowire body and cluster in part B; (D) STEM image of a single Ag nanowire at 0.50 mM $HAuCl_4$; (E) STEM image of a bright spot; (F) EDX measurement of nanowire body and cluster in part E.

bright spots in DFM images, with the size up to 217 nm are generated near the two ends of the single nanowire at low [$HAuCl_4$] (Figure S3 for more examples). Figure 3B shows that these blocks are clusters composed of smaller nanoparticles. We can also see from Figure 3B that some parts of the nanowire body become hollow as the blocks formed. The EDX measurement proves that the blocks are nearly pure Ag, whereas the nanotube is composed of both Ag and Au (Figure 3C). If we keep delivering the reactant $HAuCl_4$ into the flow cell, the whole body of nanowire will be turned into a nanotube totally.

On the other hand, these Ag blocks only appear in a certain time window but do not always exist. As Figure 2B shows, there are mainly four bright spots corresponding to the Ag blocks appearing on the nanowire. The decrease of scattering intensity indicates that the Ag blocks become smaller and smaller. Figure 2B shows that all bright spots decrease in scattering intensity and vanish especially for the two blocks at the left side indicating they vanished as the reaction goes on. According to the principle of GRR, only gold is expected to deposit on nanowire during GRR.[27,38] The structure of Au deposited nanotube has been observed by Xia and others.[29,11] These blocks have not been found in other publications mainly because their observation is not in situ and real time and reaction was in high concentration of $HAuCl_4$.[11] This may be the reason that only the nanotube is usually presented in other publications after long time reaction[29] or at higher temperature and higher concentration of $HAuCl_4$ solution than ours.[11]

The growth of such large pure Ag blocks is at the cost of consuming Ag atoms on the body of nanowire as shown in Figure 1 and Figure 2. The growth of bright spots (Ag blocks) needs reduction of large number of Ag^+. These Ag^+ come from the dissolution of the Ag nanowire during GRR. In Figure 1 and Figure 2, we can see an abrupt decrease in scattering intensity which corresponds to the formation of nanotube. The change from nanowire to nanotube only takes about 100 s as shown in Figure 2C. This means the inner part of the Ag nanowire can be corroded by $HAuCl_4$, resulting in a hollow structure very rapidly. The reaction generates a large number of Ag^+ to support the growth of the Ag blocks. Therefore, it is reasonable to state that most of the Ag have been consumed by the growth of Ag nanoblocks. The major generating of the Ag^+ does not come from the dissolution of Ag on the outside surface but comes from corrosion of the inner part of the Ag nanowire during a rapid dissolve state in our experiment. Pits and pores are formed when GRR lasts for about 1500 s, which is long enough to make the inner part of the Ag nanowire contact with $HAuCl_4$ solution as Figure S8 shows. This reaction in the inner part of the nanowire results in hollow tube as Figure 3B shows.

At high [$HAuCl_4$] (0.50 mM), the entire Ag nanowire will be covered by an assembly of numerous nanoparticles (Figure 3D and Figure 3E). The clusters of the particles near the center of nanowire have larger sizes (Figure 3F). However, the shape of these clusters of particles varies from that at low [$HAuCl_4$] in Figure 3B. The figure only exhibited a thick body of nanowire with a width up to 160 nm, which is much larger than the width of as-synthesized Ag nanowire (50.1 ± 8.5 nm). The nanowire gets wider due to the deposition of Au nanoparticles on the surface of the Ag nanowire. The EDX measurement shows that both the cluster and the body of the nanowire are composed of Ag and Au (Figure 3F).

Figure 1 and Figure 2A show that most of the bright spots, i.e., the Ag blocks, are distributed on the two ends of the nanowire in 0.02 mM $HAuCl_4$ solution. However, Figure 2E shows that more bright spots, i.e., the Au nanoparticles, appear in the middle part of nanowire at high concentration of $HAuCl_4$ compared to Figure 2A. Therefore, single Ag nanowire could show diverse bright spot distributions at different [$HAuCl_4$]s. The distribution of blocks can be explained by common crystal growth theory. It is widely accepted that the crystal growth initiated from the random nucleation.[39,40] For the unevenly distributed growth condition like our Ag nanowire, the nucleation may occur preferentially at the favorable location and depress the growth at other places. Large blocks of crystal or even the single crystal can be obtained at the favorable location. As discussed below, the growth condition affected by net surface charge will induce the distribution of the deposited particles or blocks.

3.4. Generation of Net Surface Charge on Single Ag Nanowire. According to electrostatic theory, the electric potential of a conductive material decreases with more negative charges.[5] Figure 4A clearly shows that each electrochemical potential trajectory meets a decrease after a certain time of GRR at different [$HAuCl_4$]s. Especially for 0.02 mM $HAuCl_4$, the potential exhibits a large decrease from ~0.83 to ~0.7 V at ~1500 s. Therefore, we can assume that the nanowires are injected with some negative charges. However, it is a complicated process for the negative charges to be injected into a conductive material in solution. The surface of a conductive material could carry charges through numerous modes, such as electron affinity differences of two phases, ionization of surface groups, and differential ion adsorption from electrolyte solution.[1−3] In this research, the negative charges may originate from electron affinity differences of two phases (Ag nanowire and solution with Ag^+) and the specific adsorption of Cl^-.[1,41] Owing to the electron affinity (i.e., electrochemical potential) differences of two phases, the electron could transfer from a low electron affinity phase (i.e., high electrochemical potential) to a phase with high electron

DOI: 10.1021/acs.jpcc.5b12390
J. Phys. Chem. C 2016, 120, 16608−16616

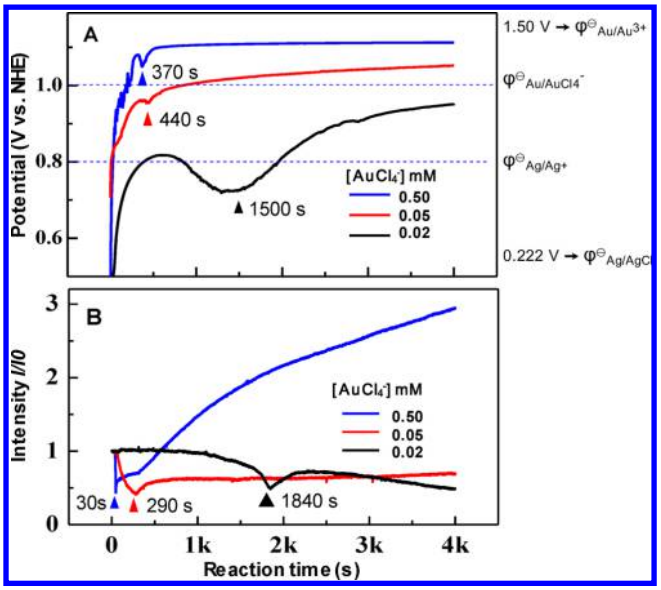

Figure 4. Electrochemical potential trajectories and intensity trajectories at different [$HAuCl_4$]s during GRR. (A) Potential trajectories of Ag nanowires. The potential in the figure is the open circuit potential (OCP). Ag nanowires were immobilized on bare Au electrode. (B) Typical intensity trajectories of single Ag nanowires.

affinity (i.e., low electrochemical potential). Therefore, AgCl can be formed through the reaction

$$Ag + Cl^- - e^- \rightarrow AgCl \qquad \varphi^{\ominus}_{Ag/AgCl} = 0.222\ V \qquad (3)$$

Actually, the potential change in Figure 4A is a mixed potential of reactions in eqs 1−3.[42] At the beginning of GRR, the reaction happens through eqs 1 and 2 very quickly, since there is a large Ag surface on Ag nanowire. Large amounts of Cl^- ions are released through the reduction of $AuCl_4^-$. Due to the very low solubility of AgCl and large fresh surface of Ag, reaction in eq 3 decreases the potential of the electrode; thus the electrochemical potential is low at the beginning of GRR. With the decrease of outside surface of Ag (deposition of Au on the surface decreases the surface area of Ag during GRR), GRR becomes slower, and the reactions in eqs 1 and 2 dominate the potential of the electrode. The electrochemical potential increases as shown in Figure 4A.

Following the increase in electrochemical potential, a decrease happens due to the formation of the pit as Figure S8 shows. As we know, the initial galvanic displacement reaction between the Ag nanowire and $HAuCl_4$ solution results in the formation Au deposited on the surface of the Ag nanowire as discussed above (see EDX on the surface of the nanowire). On the other hand, the formation of the pits on the surface of the nanowire makes the $HAuCl_4$ solution penetrate the Au shell, letting the inner part of the Ag nanowire intact with $HAuCl_4$ solution. Ag nanowire and the Au shell will form an Au−Ag junction. Electron affinity differences between metals can induce the formation of galvanic cell, i.e., a primary battery. If we consider the nanowire as a short-circuited nano primary battery, it is easy to understand why net electrons can be injected on the surface of the nanowire and decrease the OCP. The Au shell on the outside surface of the Ag nanowire acts as cathode, while the Ag in the inner part acts as anode. The resultant Au−Ag junctions perform as short-circuited nano primary batteries. The Ag in the inner part serves as the anode and is oxidized to Ag^+ ions. The Ag^+ reacted with Cl^-, forming AgCl. The redox reaction between metallic Ag and Cl^- generates an electric current that supports the continued reduction of $AuCl_4^-$ resulting in deposition of Au on the cathodic end of the nano primary battery, i.e., the outside surface of the Au shell. The dissolving in the inner part of the nanowire induces the formation of hollow nanotube as Figure 5B shows. Given that the potentials of zero charge (PZC) of

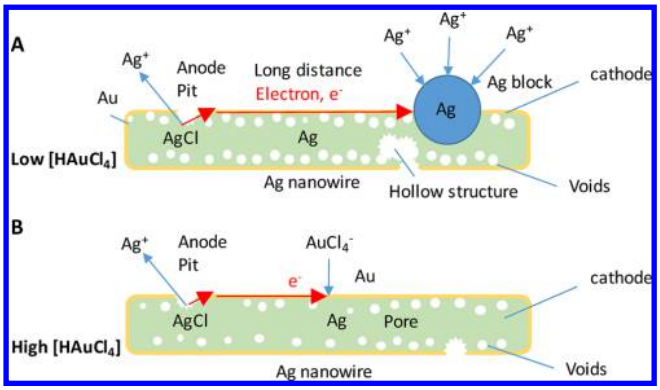

Figure 5. Schematic of the mechanism for the GRR on single Ag nanowire at different [$HAuCl_4$]s: (A) for low [$HAuCl_4$]; (B) for high [$HAuCl_4$].

Ag(111) and Ag(110) are −0.45 and −0.74 V (NHE), respectively, a fresh Ag surface (anode) could carry positive charges in the solution with Ag^+.[41]

However, the Cl^-, which specifically adsorbed on the Ag anode, comes from the GRR on the surface, resulting in the formation of AgCl. The concentration of Cl^- is usually higher than that of Ag^+ according to the two half-reactions in eqs 1 and 2 for GRR. Coupled with the adsorption of Cl^- in the inner surface of the nanowire, the anode possesses extremely high activity and could quickly convert to Ag^+ through eq 1 and AgCl through eq 3

The intensity dropping in Figure 2 and Figure 4B indicates the fast consumption of Ag on nanowire. A large number of electrons could be released through this rapid process. Since the amount of $HAuCl_4$ was much larger than Ag nanowire, the GRR could not obviously change the concentration of $HAuCl_4$. The equilibrium potential of Au is 1.000 V as shown in eq 1. Hence, the potential dropping in Figure 4A is mainly controlled by the formation of AgCl in eq 3. Such low potential will drive the reduction of Ag^+ on Ag block. The consumption of Ag of nanowire is strongly related to the potential dropping, i.e., negative charge injection. Therefore, the time of potential decrease in Figure 4A is consistent with that of scattering intensity drop in Figure 4B.

3.5. Mechanism for the GRR on Single Ag Nanowire at Different [$HAuCl_4$]s. Generally, during GRR, the redox occurs on the surface of Ag nanowires resulting in dissolving of Ag^+ and deposition of Au on the surface (Figure 5). Therefore, an Ag@Au core−shell structure formed as the first step of the structure variation.[9] Then different diffusivities of atoms between Ag and Au result in the net diffusion of Ag to the surface of nanowire, forming Au−Ag alloy shell outside the surface. At low $HAuCl_4$ concentration, the Au shell can slow down the GRR on the surface of nanowire. After certain time, some lattice vacancies or small voids in the body of the wire formed resulting in a porous structure in the Ag nanowire due to the diffusion of the Ag atoms (Figure 5A). This different diffusivity of atoms in a diffusion couple causing a super-

DOI: 10.1021/acs.jpcc.5b12390
J. Phys. Chem. C 2016, 120, 16608−16616

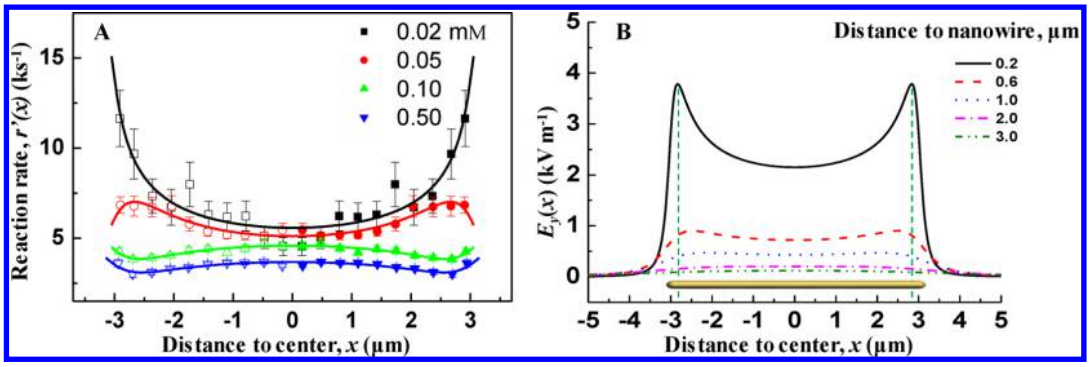

Figure 6. (A) Average growth rate of numerous bright spots along single Ag nanowires at different [$HAuCl_4$]. The curves show the fitting. The left side of the origin of coordinates is the image at the right side. The length of all nanowires is normalized to an average length of 6.3 μm. Error bar shows the standard deviation. The number of nanowires for each [$HAuCl_4$] is larger than 50. (B) Simulation of $E_y(x)$ around a nanowire with 6.3 μm (see Supporting Information section SI.5 for details of simulation).

saturation of lattice vacancies is called the Kirkendall effect.[12] The porous structure with large number of void surface makes it very easy to be corroded by $HAuCl_4$. But the porous active Ag is sealed by the Au shell. Fortunately, the forming of pit or pinhole on the surface of the Au shell made the porous structure contact with the $HAuCl_4$ solution. The formation of the pit or pinhole has been widely observed in other research.[9]

As discussed in section 3.4, nano primary batteries can be formed between the Au shell and the porous Ag inner part. Due to the structure of nano primary battery, the redox reaction between metallic Ag and Cl^- ion generates an electric current that supports the continued growth of the cathodic end of the nano primary battery. On the cathode end (Au shell), the net electrons were generated on it since the electric current flow into the surface of the nanowire from the inner surface. In the solution with low $HAuCl_4$ concentration, the $AuCl_4^-$ ions are reduced with a rapid rate, resulting in Au deposition on the surface of the outside surface of the nanowire (cathode). This reaction exhausts the $AuCl_4^-$ during the rapid reaction since the delivery of $HAuCl_4$ solution is at low rate of 10 μL/min. This rapid reaction can be identified by the abrupt decrease of scattering intensity at about 1800 s as shown in Figure 2B. The abrupt decrease in light scattering intensity indicates an abrupt change from a nanowire to a nanotube, as Figure 2B shows. This abrupt change from nanowire to nanotube results in rapid dissolving of Ag at the inner surface of the nanowire (anode). Therefore, a large amount of electrons can be generated and flow to the outside surface of the nanowire, resulting in rapid reduction of $AuCl_4^-$ at cathode end. Thus, $AuCl_4^-$ has been exhausted by this rapid reaction. This exhaustion lasts only for a short time. Therefore, the reduction of $AuCl_4^-$ is stopped by this exhaustion. But the structure of nano primary battery still exists (the nanowire has not totally turn into nanotube, as Figure 5B shows). Accumulation of electrons on the cathode will induce reduction of Ag^+ to Ag nanoblock. Three Ag^+ are formed coupled with reduction of one Au atom; therefore there are excessive Ag^+ species to support the growth of the large Ag blocks. That is why Ag nanoblocks formed on the surface of the nanowire in 0.02 mM $HAuCl_4$.

At high reaction rate, $HAuCl_4$ is consumed quickly at anode (inner surface of the porous Ag surface) and reactions 1 and 3 become the dominant reactions (Figure 5A). The cell potential between reactions 1 and 3 at T = 293 K is as large as 0.577 V, which indicates that both reactions 1 and 3 can happen on the same Ag nanowire simultaneously. At this moment, the Ag nanowire still has a porous and active structure, which implies that both reactions 1 and 3 can happen at high reaction rate.

The growth of the void induces the mass loss of the nanowire, while the growth of the Ag blocks increases the total mass. Therefore, the process induces the mass transport from the body of Ag nanowire to Ag blocks. The transportation is a far distance and electron coupled process, which is induced by the transfer of the Ag^+ through diffusion in the solution and the electrons transfer along the surface of the nanowire. The electrons and the Ag^+ recombined forming the Ag blocks on the surface (Figure 5A).

However, the rapid reaction (critical intermediate state) only lasts a very short time. The Ag blocks will stop growing when the critical state is terminated. As the nanowire turns totally to nanotube, i.e., pure Ag beneath the Au shell has been exhausted; the structure of the nano primary batteries is destroyed. Thus, the generation of the electron current stops. But the GRR will not stop until an equilibrium state is reached. The pure Ag blocks will redissolve into the solution due to the corrosion by $HAuCl_4$, which is keeping delivery into the flow cell at the rate of 10 μL/min. The smaller ones usually dissolve faster, while it will take a longer time for larger ones to dissolve as shown in Figure 1E.

At high $HAuCl_4$ concentration, different from the exhaustion of $HAuCl_4$ at low concentration, $HAuCl_4$ cannot be exhausted by the rapid reaction. Therefore, $AuCl_4^-$ was reduced and deposited on the outside surface of the nanowire inducing deposition of Au nanoparticles rather than Ag. The driving force is high enough that the reaction occurs all over the nanowire with much less selectivity (Figure 5B). We can assume that the $AuCl_4^-$ concentration does not change much, although the reaction rate is very fast. Reactions 1 and 2 will dominate the reactions on the outside surface and the inner surface of the nanowire, respectively, and the deposition of Ag will not happen.

3.6. Model for Net Surface Charge Controlled GRR at Different [$HAuCl_4$]s. Nanoparticles with certain shapes or structures usually present different facets,[43] defects,[32−34] and ligand/surfactant coverage[28,44] at different locations. These specific local properties could determine the local reaction activity on a single nanoparticle. Hence, nanoparticles with different shapes and structures generally show unevenly distributed activity.[10,32−34,43] To improve the performance of nanoparticles, knowledge of which locations are more active and what exact properties drive the diverse activity patterns is necessary. However, among these properties, the contribution

DOI: 10.1021/acs.jpcc.5b12390
J. Phys. Chem. C 2016, 120, 16608−16616

of net surface charge on a single nanoparticle in the unevenly distributed activity is rarely investigated.

Figure 6A shows the average growth rate of numerous bright spots along single Ag nanowires at different [$HAuCl_4$]s. The average growth rate near the two ends is considerably higher than that in the middle at low [$HAuCl_4$], whereas the trend is opposite at high [$HAuCl_4$]. This observation is consistent with the results in Figure 2 and Figure 3.

Owing to the existence of the electric double layer around the single nanowire, the homocharges on nanowire can repel each other. According to the electrostatic theory, the two ends of the nanowire will have higher charge density ($\sigma(x)$).[4] The intensity of electric field in the y direction ($E_y(x)$) generated by the net surface charges will be stronger near the two ends than the center (Figure 6B). The static electric field causes a field-induced mass transport[6,7] and affects the chemical reactions on the nanomaterial. Moreover, the simulation in Figure 6B shows that the strongest value of $E_y(x)$ appears near the ends but not at the ends of nanowire. A similar finding is observed in the bright spots with higher activity.

Therefore, a model could be derived for GRR on single Ag nanowire at low and high [$HAuCl_4$] (Figure 7). Single Ag

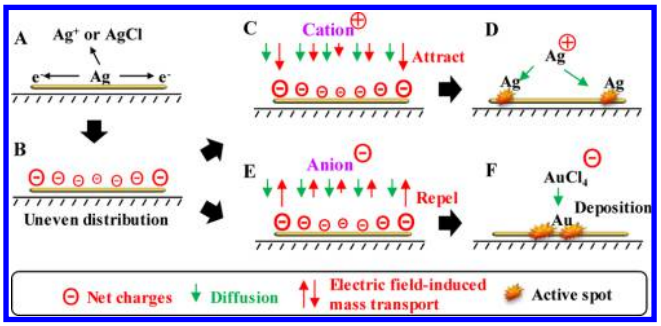

Figure 7. Schematic of the reduction reactions of cation and anion on a nanowire. (A) Charge of a single Ag nanowire. (B) Unevenly distributed net surface charge. (C) Directions of diffusion-induced and electric field-induced mass transport are same for cation. (D) More reactions near the two ends. (E) Directions are opposite for anion. (F) More reactions in the middle part.

nanowire will carry certain net surface charges through the oxidation of Ag or adsorption of Cl^- (Figure 7A,B). The two ends of the nanowire possess more charges than the middle part because of the repulsion between homocharges through the electric double layer around the nanowire. At low [$HAuCl_4$], cations, such as Ag^+, will be attracted to the two ends and consequently accomplish greater Ag^+ reduction near the ends (Figure 6A and Figure 7C,D). Therefore, we can see that the unevenly distributed electrons could induce the uneven distribution of Ag^+, resulting in the reduction of Ag^+ near the end.

Given that the strongest value of $E_y(x)$ appears near the ends of the single nanowire (Figure 6B), the bright spots usually grow faster near the ends but not at the ends (Figure 2A and Figure 3A). At high [$HAuCl_4$], the anion, such as $AuCl_4^-$, will be repelled by the net surface charge on nanowire and will be difficult to diffuse to the nanowire. If the ends of nanowire carry more negative charges, the anion will be more difficult to diffuse to the ends of nanowire (Figure 7E). In consequence, the two ends of nanowire will show lower activity than the middle part (Figure 3D, Figure 6A, and Figure 7F). Therefore, unevenly distributed net surface charges can induce the activity variation of the nanomaterial.[13,14]

On the basis of the discussion above, a mathematic model for the growth rate of bright spots is built (see Supporting Information section SI.5 for details).

$$r(x) = (\mu_{Ag^+}[Ag^+]^{H_d} - \mu_{AuCl_4^-}[AuCl_4^-]^{H_d})E_y(x) - D_{Ag^+}\frac{d[Ag^+]}{dy} - D_{AuCl_4^-}\frac{d[AuCl_4^-]}{dy} \quad (4)$$

where $r(x)$ is the reduction reaction rate and μ, D, and H_d are the ion mobility, diffusion coefficient, and thickness of diffusion layer, respectively. Moreover, the reaction rate $r(x)$ is proportional to the change rate of scattering intensity,[45]

$$r'(x) = \langle \Delta I(x)/\Delta t \rangle \propto r(x) \quad (5)$$

The model above can fit the experimental data in Figure 6A well (Supporting Information section SI.5 for details). Qualitatively, the term $(\mu_{Ag^+}[Ag^+]^{H_d} - \mu_{AuCl_4^-}[AuCl_4^-]^{H_d})$ could be a positive or negative value at different [$HAuCl_4$]s, and consequently, $r'(x)$ will show different distributions in Figure 6A. Besides the effect of net surface charge, other common possible reasons, including facets, defects, surfactant, surface plasmon resonance, postripening process, and diffusion, are found to be unrelated to the unevenly distributed activity (Supporting Information section SI.6 for details).

4. CONCLUSION

We use ions as probes to detect the distribution of net surface charge and track galvanic replacement reaction on single Ag nanowire in situ and in real time by dark-field microscopy. The research reveals that the unevenly distributed net surface charge performs multifunctions in determining reaction selectivity, product shape, and activity distribution. The two ends of a single Ag nanowire possess more net surface charges than the middle part. Owing to the interaction between the net surface charges and ions in solution, many clusters are found to be generated on the Ag nanowires. These clusters are the locations where faster deposition reaction happens. Furthermore, larger size Ag blocks with clear shape are produced near the two ends by attracting Ag^+ at lower [$HAuCl_4$], but larger size Ag–Au alloy clusters with veiled shape are produced near the center by repelling $AuCl_4^-$ at higher [$HAuCl_4$]. Net surface charge widely exists in the fields of nanoscience, such as nanosynthesis,[28,46,47] electrochemistry,[13] photo(photoelectro)chemistry,[14] and catalysis.[15] The methodology and knowledge from this research can be widely applied to other reactions and other shaped nanomaterials.

■ ASSOCIATED CONTENT

Supporting Information

The Supporting Information is available free of charge on the ACS Publications website at DOI: 10.1021/acs.jpcc.5b12390.

Additional details on experiment design, control experiment, figures, and simulations (PDF)
Ag nanowires from 0 to ~5 ks (AVI)
Ag nanowires from 0 to ~2 ks (AVI)

■ AUTHOR INFORMATION

Corresponding Author

*E-mail: xczhou2013@sinano.ac.cn.

DOI: 10.1021/acs.jpcc.5b12390
J. Phys. Chem. C 2016, 120, 16608–16616

Notes

The authors declare no competing financial interest.

■ ACKNOWLEDGMENTS

This work was supported by the National Natural Science Foundation of China (Grants 21373264 and 21573275), the Natural Science Foundation of Jiangsu Province (Grant BK20150362), Suzhou Institute of Nano-Tech and Nano-Bionics (Grant Y3AAA11004), and Thousand Youth Talents Plan (Grant Y3BQA11001). We are also thankful to Jinping Zhang and Xuehua Liu for their help on TEM and EDX measurements.

■ REFERENCES

(1) Bard, A. J.; Faulkner, L. R. *Electrochemical Methods: Fundamentals and Applications*, 2nd ed.; John Wiley & Sons Inc., 2001.
(2) Fisher, L. H.; Varney, R. N. Contact Potentials Between Metals: History, Concepts, and Persistent Misconceptions. *Am. J. Phys.* **1976**, *44*, 464−475.
(3) Khan, S. U. M.; Kainthla, R. C.; Bockris, J. O. M. The Redox Potential and the Fermi Level in Solution. *J. Phys. Chem.* **1987**, *91*, 5974−5977.
(4) Griffiths, D. J.; Li, Y. Charge Density on a Conducting Needle. *Am. J. Phys.* **1996**, *64*, 706−714.
(5) Smythe, W. R. *Static and Dynamic Electricity*; Hemisphere: New York, 1989.
(6) Zhao, J.; Huang, J.-Q.; Wei, F.; Zhu, J. Mass Transportation Mechanism in Electric-Biased Carbon Nanotubes. *Nano Lett.* **2010**, *10*, 4309−4315.
(7) Bologa, M. K.; Grosu, F. P. Enhancement of Heat and Mass Transfer by an Electric Field. *Surf. Engin. Appl.Electrochem.* **2012**, *48*, 456−464.
(8) Wiley, B.; Sun, Y. G.; Mayers, B.; Xia, Y. N. Shape-controlled Synthesis of Metal Nanostructures: The Case of Silver. *Chem. - Eur. J.* **2005**, *11*, 454−463.
(9) Sun, Y.; Wang, Y. Monitoring of Galvanic Replacement Reaction between Silver Nanowires and HAuCl4 by In Situ Transmission X-ray Microscopy. *Nano Lett.* **2011**, *11*, 4386−4392.
(10) Shen, Y.; He, T.; Wang, W.; Zhan, Y.; Hu, X.; Yuan, B.; Zhou, X. Fluorescence Enhancement on Silver Nanoplates at the Single- and Sub-nanoparticle Level. *Nanoscale* **2015**, *7*, 20132−20141.
(11) Sun, Y.; Xia, Y. Mechanistic Study on the Replacement Reaction between Silver Nanostructures and Chloroauric Acid in Aqueous Medium. *J. Am. Chem. Soc.* **2004**, *126*, 3892−3901.
(12) Fan, H. J.; Gösele, U.; Zacharias, M. Formation of Nanotubes and Hollow Nanoparticles Based on Kirkendall and Diffusion Processes: A Review. *Small* **2007**, *3*, 1660−1671.
(13) Zhang, L.; Henkelman, G. Tuning the Oxygen Reduction Activity of Pd Shell Nanoparticles with Random Alloy Cores. *J. Phys. Chem. C* **2012**, *116*, 20860−20865.
(14) Gao, H.; Liu, C.; Jeong, H. E.; Yang, P. Plasmon-Enhanced Photocatalytic Activity of Iron Oxide on Gold Nanopillars. *ACS Nano* **2012**, *6*, 234−240.
(15) Hahn, C. Enhancing Electrophilic Alkene Activation by Increasing the Positive Net Charge in Transition-metal Complexes and Application in Homogeneous Catalysis. *Chem.—Eur. J.* **2004**, *10*, 5888−5899.
(16) Zhang, Y.; Kolmakov, A.; Chretien, S.; Metiu, H.; Moskovits, M. Control of Catalytic Reactions at the Surface of a Metal Oxide Nanowire by Manipulating Electron Density Inside It. *Nano Lett.* **2004**, *4*, 403−407.
(17) Jaquith, M. J.; Anthony, J. E.; Marohn, J. A. Long-lived Charge Traps in Functionalized Pentacene and Anthradithiophene Studied by Time-resolved Electric Force Microscopy. *J. Mater. Chem.* **2009**, *19*, 6116−6123.
(18) Johnson, A. S.; Nehl, C. L.; Mason, M. G.; Hafner, J. H. Fluid Electric Force Microscopy for Charge Density Mapping in Biological Systems. *Langmuir* **2003**, *19*, 10007−10010.
(19) Wu, Y.; Wang, D.; Zhou, G.; Yu, R.; Chen, C.; Li, Y. Sophisticated Construction of Au Islands on Pt-Ni: An Ideal Trimetallic Nanoframe Catalyst. *J. Am. Chem. Soc.* **2014**, *136*, 11594−11597.
(20) Gao, C.; Lu, Z.; Liu, Y.; Zhang, Q.; Chi, M.; Cheng, Q.; Yin, Y. Highly Stable Silver Nanoplates for Surface Plasmon Resonance Biosensing. *Angew. Chem., Int. Ed.* **2012**, *51*, 5629−5633.
(21) Wang, Y.; Liu, Y.; Luehmann, H.; Xia, X.; Wan, D.; Cutler, C.; Xia, Y. Radioluminescent Gold Nanocages with Controlled Radioactivity for Real-Time in Vivo Imaging. *Nano Lett.* **2013**, *13*, 581−585.
(22) Chen, J.; McLellan, J. M.; Siekkinen, A.; Xiong, Y.; Li, Z.-Y.; Xia, Y. Facile Synthesis of Gold-silver Nanocages with Controllable Pores on the Surface. *J. Am. Chem. Soc.* **2006**, *128*, 14776−14777.
(23) Chen, J.; Wiley, B.; McLellan, J.; Xiong, Y.; Li, Z.-Y.; Xia, Y. Optical Properties of Pd−Ag and Pt−Ag Nanoboxes Synthesized via Galvanic Replacement Reactions. *Nano Lett.* **2005**, *5*, 2058−2062.
(24) Moon, G. D.; Choi, S.-W.; Cai, X.; Li, W.; Cho, E. C.; Jeong, U.; Wang, L. V.; Xia, Y. A New Theranostic System Based on Gold Nanocages and Phase-Change Materials with Unique Features for Photoacoustic Imaging and Controlled Release. *J. Am. Chem. Soc.* **2011**, *133*, 4762−4765.
(25) Sun, Y.; Mayers, B.; Herricks, T.; Xia, Y. Polyol Synthesis of Uniform Silver Nanowires: A Plausible Growth Mechanism and the Supporting Evidence. *Nano Lett.* **2003**, *3*, 955−960.
(26) Sun, Y.; Mayers, B. T.; Xia, Y. Template-Engaged Replacement Reaction: A One-Step Approach to the Large-Scale Synthesis of Metal Nanostructures with Hollow Interiors. *Nano Lett.* **2002**, *2*, 481−485.
(27) Sun, Y.; Wiley, B.; Li, Z.-Y.; Xia, Y. Synthesis and Optical Properties of Nanorattles and Multiple-Walled Nanoshells/Nanotubes Made of Metal Alloys. *J. Am. Chem. Soc.* **2004**, *126*, 9399−9406.
(28) Sun, Y.; Yin, Y.; Mayers, B. T.; Herricks, T.; Xia, Y. Uniform Silver Nanowires Synthesis by Reducing AgNO3 with Ethylene Glycol in the Presence of Seeds and Poly(Vinyl Pyrrolidone). *Chem. Mater.* **2002**, *14*, 4736−4745.
(29) Xia, X.; Wang, Y.; Ruditskiy, A.; Xia, Y. 25th Anniversary Article: Galvanic Replacement: A Simple and Versatile Route to Hollow Nanostructures with Tunable and Well-Controlled Properties. *Adv. Mater.* **2013**, *25*, 6313−6333.
(30) Zhang, H.; Jin, M.; Liu, H.; Wang, J.; Kim, M. J.; Yang, D.; Xie, Z.; Liu, J.; Xia, Y. Facile Synthesis of Pd−Pt Alloy Nanocages and Their Enhanced Performance for Preferential Oxidation of CO in Excess Hydrogen. *ACS Nano* **2011**, *5*, 8212−8222.
(31) Smith, J. G.; Yang, Q.; Jain, P. K. Identification of a Critical Intermediate in Galvanic Exchange Reactions by Single-Nanoparticle-Resolved Kinetics. *Angew. Chem., Int. Ed.* **2014**, *53*, 2867−2872.
(32) Zhou, X.; Andoy, N. M.; Liu, G.; Choudhary, E.; Han, K.-S.; Shen, H.; Chen, P. Quantitative Super-resolution Imaging Uncovers Reactivity Patterns on Single Nanocatalysts. *Nat. Nanotechnol.* **2012**, *7*, 237−241.
(33) Blythe, K. L.; Titus, E. J.; Willets, K. A. Triplet-State-Mediated Super-Resolution Imaging of Fluorophore-Labeled Gold Nanorods. *ChemPhysChem* **2014**, *15*, 784−793.
(34) Tachikawa, T.; Yamashita, S.; Majima, T. Evidence for Crystal-Face-Dependent TiO2 Photocatalysis from Single-Molecule Imaging and Kinetic Analysis. *J. Am. Chem. Soc.* **2011**, *133*, 7197−7204.
(35) Rust, M. J.; Bates, M.; Zhuang, X. Sub-diffraction-limit Imaging by Stochastic Optical Reconstruction Microscopy (STORM). *Nat. Methods* **2006**, *3*, 793−795.
(36) Betzig, E.; Patterson, G. H.; Sougrat, R.; Lindwasser, O. W.; Olenych, S.; Bonifacino, J. S.; Davidson, M. W.; Lippincott-Schwartz, J.; Hess, H. F. Imaging Intracellular Fluorescent Proteins at Nanometer Resolution. *Science* **2006**, *313*, 1642−1645.
(37) Zhou, X.; Choudhary, E.; Andoy, N. M.; Zou, N.; Chen, P. Scalable Parallel Screening of Catalyst Activity at the Single-Particle Level and Subdiffraction Resolution. *ACS Catal.* **2013**, *3*, 1448−1453.

DOI: 10.1021/acs.jpcc.5b12390
J. Phys. Chem. C 2016, 120, 16608−16616

(38) Bernard Ng, C. H.; Tan, H.; Fan, W. Y. Formation of Ag2Se Nanotubes and Dendrite-like Structures from UV Irradiation of a CSe2/Ag Colloidal Solution. *Langmuir* **2006**, *22*, 9712−9717.
(39) VanSiclen, C. D. Random Nucleation and Growth Kinetics. *Phys. Rev. B: Condens. Matter Mater. Phys.* **1996**, *54*, 11845−11848.
(40) Trojanek, A.; Langmaier, J.; Samec, Z. Random Nucleation and Growth of Pt Nanoparticles at the Polarised Interface between Two Immiscible Electrolyte Solutions. *J. Electroanal. Chem.* **2007**, *599*, 160−166.
(41) Parsons, R. The Electrical Double Layer: Recent Experimental and Theoretical Developments. *Chem. Rev.* **1990**, *90*, 813−826.
(42) Park, J. H.; Zhou, H.; Percival, S. J.; Zhang, B.; Fan, F.-R. F.; Bard, A. J. Open Circuit (Mixed) Potential Changes Upon Contact Between Different Inert Electrodes-Size and Kinetic Effects. *Anal. Chem.* **2013**, *85*, 964−970.
(43) Zhang, Q.; Wang, H. Facet-Dependent Catalytic Activities of Au Nanoparticles Enclosed by High-Index Facets. *ACS Catal.* **2014**, *4*, 4027−4033.
(44) Duan, H.; Wang, D.; Li, Y. Green Chemistry for Nanoparticle Synthesis. *Chem. Soc. Rev.* **2015**, *44*, 5778−5792.
(45) Ni, W. H.; Ba, H. J.; Lutich, A. A.; Jackel, F.; Feldmann, J. Enhancing Single-Nanoparticle Surface-Chemistry by Plasmonic Overheating in an Optical Trap. *Nano Lett.* **2012**, *12*, 4647−4650.
(46) Li, X.; Lian, J.; Lin, M.; Chan, Y. Light-Induced Selective Deposition of Metals on Gold-Tipped CdSe-Seeded CdS Nanorods. *J. Am. Chem. Soc.* **2011**, *133*, 672−675.
(47) Habas, S. E.; Yang, P.; Mokari, T. Selective Growth of Metal and Binary Metal Tips on CdS Nanorods. *J. Am. Chem. Soc.* **2008**, *130*, 3294−3295.

DOI: 10.1021/acs.jpcc.5b12390
J. Phys. Chem. C 2016, 120, 16608−16616